Thermodynamic study of sodium–iron oxides
Part II. Ternary phase diagram of the Na–Fe–O system

Jintao Huang[*], Tomohiro Furukawa, Kazumi Aoto

*Oarai Engineering Center, Japan Nuclear Cycle Development Institute, Narita-cho 4002,
Oarai-machi, Ibaraki-ken 311-1393, Japan*

Abstract

Studies on ternary phase diagrams of the Na–Fe–O system have been carried out from the thermodynamic point of view. Thermodynamic data of main ternary Na–Fe oxides $Na_4FeO_3(s)$, $Na_3FeO_3(s)$, $Na_5FeO_4(s)$ and $Na_8Fe_2O_7(s)$ have been assessed. A user database has been created by reviewing literature data together with recent DSC and vapor pressure measurements by the present authors. New ternary phase diagrams of the Na–Fe–O system have been constructed from room temperature to 1000 K. Stable conditions of the ternary oxides at 800 K were presented in predominance diagram as functions of oxygen pressure and sodium pressure.
© 2003 Elsevier Science B.V. All rights reserved.

Keywords: Na–Fe–O system; Phase diagram; Thermodynamics

1. Introduction

Many pioneers have studied ternary phase diagrams of the Na–Fe–O system but there still exist discrepancies. Early phase diagram study on the Na–Fe–O system had been done by Dai et al. [1,2]. Some isothermal phase diagrams of $FeO(s)–Na_2O(s)$, $FeO(s)–Na_2Fe_2O_4(s)$ and $Fe_3O_4(s)–Na_2Fe_2O_4(s)$ were given. Lindemer et al. [3] constructed ternary Na–Fe–O phase diagram and Ellingham diagram in which $Na_2FeO_2(s)$, $Na_8Fe_2O_7(s)$, $Na_3Fe_5O_9(s)$ as well as $Na_4Fe_6O_{11}(s)$, were included by using estimated thermodynamic data. Their work correctly predicted the formation of $Na(l)–Fe(s)–Na_4FeO_3(s)$ at high temperatures though stability of some ternary oxides involved had not been confirmed. Partial phase

diagram at low oxygen potentials and oxygen–sodium potential diagram at 853 K were presented by Seetharaman and Du [4]. Possibility of formation of $Na_2FeO_2(s)$ was ruled out by them by thermodynamic analysis. Sridharan et al. [5,6] did extensive experiments by thermal analysis, solid-state reactions, etc. . . . so that partial phase diagram over 773 K was deduced. However, large discrepancy can be found among the available phase diagrams mentioned above. For example, Sridharan et al. suggested that there exist two-phase lines $Na_4FeO_3(s)–Na_3FeO_3(s)$ and $Na_3FeO_3(s)–NaFeO_2(s)$ in 500–650 °C, while Seetharaman et al. reported $Na_4FeO_3(s)–NaFeO_2(s)$ and $Na_2O(s)–NaFeO_2(s)$ two-phase lines within the same temperature zone. Therefore, vapor pressure measurements on some Na–Fe oxides and DSC thermal analysis were done in the present laboratory. Thermodynamic functions of Na_3FeO_3 and Na_4FeO_3 were evaluated once again. A user database was created by reviewing thermodynamic data of other Na–Fe oxides

---

* Corresponding author. Tel.: +81-29-267-4141x5928;
fax: +81-29-267-7148.
E-mail address: huang@oec.jnc.go.jp (J. Huang).

in literatures. Thus, new ternary phase diagrams and chemical potential diagrams in the Na–Fe–O system were constructed from room temperature to 1000 K by using the Thermo-Calc code. Stability of the ternary oxides was quantitatively discussed.

2. Thermodynamic aspects

Thermodynamic basis of equilibrium calculation and the construction of phase diagram by the Thermo-Calc can be found in literature [7] as well as the User's guide. Present study employed TERN-module to create the ternary phase diagrams of the Na–Fe–O system. POLY-module was used to generate the potential diagram. The SSUB database provided by SGTE is employed as the main database for the calculation. A user database was built up for the calculation. Thermodynamic data source and assessment of literatures and experimental results are given as the following.

2.1. Binary system in Na–Fe–O

2.1.1. Na–O system

A schematic binary Na–O phase diagram can be found in literature [8]. The three binary oxides in the system, $Na_2O(s)$, $Na_2O_2(s)$ and $NaO_2(s)$, were taken into account in the present calculation but no solutions were included for lack of necessary data.

2.1.2. Fe–O system

This system is extensively investigated so that original data given in the SSUB database were utilized for the calculation, in which the three well-known solid solutions, Hematite, Magnetite and Wustite were included. Further discussion in this part is no longer necessary.

2.1.3. Na–Fe system

No further treatment was done for this binary system because no compounds were found and only very limited solutions were reported.

2.2. Ternary Na–Fe oxides

2.2.1. $NaFeO_2(s)$

Data assessed by SGTE was used. Thermodynamic data of $NaFeO_2(s)$ used for the present calculation are given in detail in Table 1 together with other ternary Na–Fe oxides. The Gibbs energy of formation of $NaFeO_2(s)$ can be expressed as,

$$\Delta_f G^\circ(Na_4FeO_3) = -701849.4 + 204.19 \times T \quad (1)$$

2.2.2. $Na_4FeO_3(s)$

This compound has been studied so many times that thermodynamic evaluation are possible. Among the available data of $Na_4FeO_3(s)$, Bhat and Borgstedt's result [9] seems more reliable because their result agrees quite well with experimental data given by Gross and Wilson [10] and Shaiu et al. [11]. Therefore, the fol-

Table 1
Thermodynamic data used for the Na–Fe–O phase diagram calculation

	NaFeO$_2$	Na$_4$FeO$_3$	Na$_3$FeO$_3$	Na$_5$FeO$_4$	Na$_8$Fe$_2$O$_7$
$\Delta_f G^\circ(298)\,\mathrm{kJ\,mol^{-1}}$	−639.98	−1107.52	−1068.3	−1462.7	−2524.3
$\Delta_f H^\circ(298)\,\mathrm{kJ\,mol^{-1}}$	−698.18	−1206.13	−1162.6	−1596.0	−2746.0
$S^\circ(298)\,\mathrm{J\,mol^{-1}\,K^{-1}}$	88.3	208.9	172.0	246.3	438.1
$C_p(T) = a + b \times T − c/T^2$ (J mol^{-1} K^{-1})					
a	100.77	212.49	181.7	262.61	444.3
b	0.0186	0.0383	0.03339	0.04818	0.08156
c	1479000	3280000	2967000	4455000	7422000
$G(T) = −g_1 + g_2 \times T − g_3 \times T \times \ln(T) − g_4 \times T^2 + g_5/T$ (J mol^{-1})					
g_1	723394	1282201	1228246	1691381	2906986
g_2	455.159	1244.166	1071.530	1551.917	2603.706
g_3	80.55	212.49	181.69	262.60	444.3
g_4	0.006653	0.019155	0.016695	0.024000	0.04078
g_5	0.0	1642000	1483500	2228000	3711000

lowing expression is employed in the present study.

$$\Delta_f G^\circ (\text{Na}_4\text{FeO}_3) = -1212202 + 351.10 \times T \qquad (2)$$

Since experimental data, such as heat capacities, enthalpy increments and Gibbs energy functions of $\text{Na}_4\text{FeO}_3(s)$ are not available, estimated data have to be used. So, Lindemer's estimation of entropy $S^\circ (298) = 208.9 \, \text{J mol}^{-1}\,\text{K}^{-1}$ was employed. Heat capacity $C_p(T)$ given by MALT2 database [12] was employed that was estimated from those of its component oxides. $\Delta_f H^\circ (298)$ was calculated according to the following formula:

$$\Delta_f H^\circ (298) = \Delta_f G^\circ (298) + T \, \Delta_f S^\circ (298) \qquad (3)$$

Thermal analysis on this compound by DSC carried out in the present laboratory shows that the melting point is around $1008 \pm 15 \, \text{K}$. No other phase transitions were found up to its melting point. Property of its liquid phase is not determined so the whole calculation was done below its melting point.

2.2.3. Na$_3$FeO$_3$(s)

Experimental measurement on this compound was very scarce. The vapor pressure measurements by the present authors provided its Gibbs energy of formation [13], as expressed in the following:

$$\Delta_f G^\circ (\text{Na}_3\text{FeO}_3) = -1168629 + 338.34 \times T \qquad (4)$$

The expression should be valid until about $1000 \, \text{K}$ because no phase transition was observed till $1033 \, \text{K}$ by DSC and XRD analysis. Similar treatments were made to estimate $S^\circ (298)$, $C_p(T)$ and $\Delta_f H^\circ (298)$ of $\text{Na}_3\text{FeO}_3(s)$ as expressed above.

2.2.4. Na$_5$FeO$_4$(s)

Thermal analysis in the present laboratory shows that there are no phase transitions for this compound from room temperature to $1000 \, \text{K}$. Up to date, experimentally measured results of $\Delta_f G^\circ (\text{Na}_5\text{FeO}_4)$ have been seldom reported in publications. Thermodynamic data for this compound, $\Delta_f H^\circ (298) = -1596 \, \text{kJ mol}^{-1}$, $S^\circ (298) = 246.3 \, \text{J mol}^{-1}\,\text{K}^{-1}$ were employed according to Lindemer's estimation while heat capacity was estimated in the similar way as described above.

$$\Delta_f G^\circ (\text{Na}_5\text{FeO}_4) = -1602430 + 467.3 \times T \qquad (5)$$

2.2.5. Na$_8$Fe$_2$O$_7$

The standard enthalpy of formation was given as $\Delta_f H^\circ (\text{Na}_8\text{Fe}_2\text{O}_7) = -2746.0 \, \text{kJ mol}^{-1}$ by Stuve et al. [14]. Lindemer et al. estimated the entropy of $\text{Na}_8\text{Fe}_2\text{O}_7$ as about $S^\circ (298) = 438.1 \, \text{J mol}^{-1}\,\text{K}^{-1}$. So, $\Delta_f H^\circ (\text{Na}_8\text{Fe}_2\text{O}_7)$ was able to be calculated by Eq. (2), i.e. $\Delta_f H^\circ (298) = -2524.3 \, \text{kJ mol}^{-1}$. Its heat capacity was roughly calculated from those of $\text{Na}_3\text{FeO}_3(s)$ and $\text{Na}_5\text{FeO}_4(s)$.

$$\Delta_f G^\circ (\text{Na}_8\text{Fe}_2\text{O}_7) = -2754068 + 771.86 \times T \qquad (6)$$

2.2.6. Na$_2$FeO$_2$(s) and other higher order oxides

It is reasonable to exclude $\text{Na}_2\text{FeO}_2(s)$ from the present calculation since experimental attempts to produce this phase failed and theoretic analysis suspected its stability [4–6]. Though some higher order Na–Fe oxides, such as $\text{Na}_3\text{Fe}_5\text{O}_9$, $\text{Na}_4\text{Fe}_6\text{O}_{11}$, $\text{Na}_{10}\text{Fe}_{16}\text{O}_{29}$ and $\text{Na}_{34}\text{Fe}_8\text{O}_{29}$ had been reported [3], they were observed neither in the present laboratory nor in Sridharan's. So, these compounds were not considered in the present calculation too.

3. Calculated phase diagrams and discussion

By means of Thermo-Calc code, new chemical potential diagram and ternary Na–Fe–O phase diagram were constructed up to about $1000 \, \text{K}$. Isothermal sections of the ternary phase diagram were illustrated in Figs. 1–6.

The partial phase diagram in the region of Na(l)–$\text{Na}_4\text{FeO}_3(s)$–$\text{Na}_3\text{FeO}_3(s)$–Fe(s) over $693 \, \text{K}$ is identical with the schematic diagram drawn by Sridharan et al. [5,6] as shown in Figs. 4–6. It indicates that the present theoretic study agrees well with their experimental results. Outside the above zone, formation of $\text{Na}_8\text{Fe}_2\text{O}_7(s)$ over about $637 \, \text{K}$ is thermodynamically favorable according to this calculation. This prediction should be consistent with that of Lindemer's at higher temperatures if $\text{Na}_2\text{FeO}_2(s)$ were excluded from their study.

Due to the importance in nuclear industry, special attention was paid to low oxygen potentials. $\text{Na}_4\text{FeO}_3(s)$ is considered as one of the main corrosion products in the sodium-leak incident of the MONJU FBR. In this calculation, it is found that Na(l), Fe(s) and $\text{Na}_4\text{FeO}_3(s)$ coexist over $694 \, \text{K}$ and
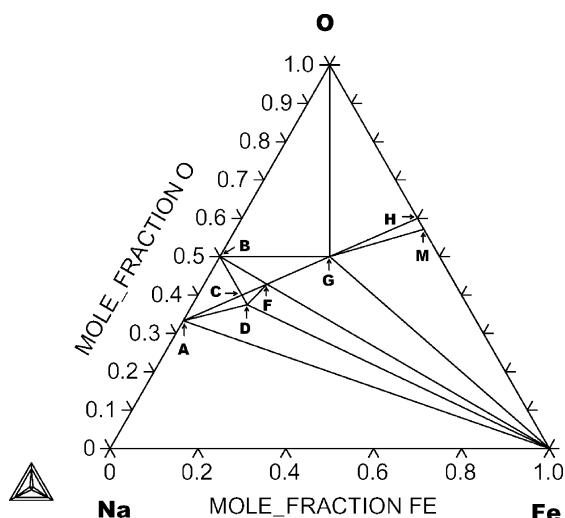
Fig. 1. Isothermal cross-sections of the Na–Fe–O ternary phase diagram in 298–536 K. (A) Na_2O; (B) Na_2O_2; (C) Na_5FeO_4; (D) Na_4FeO_3; (F) Na_3FeO_3; (G) $NaFeO_2$; (H) Hematite; (M) Magnetite.

Na(l)–Na_2O(s)–Fe(s) is more stable at lower temperatures. The calculated transition temperature is much higher than 629 K found by Sridharan et al. [15] but quite close to the 723 K reported by Bhat and Borgstedt [9].
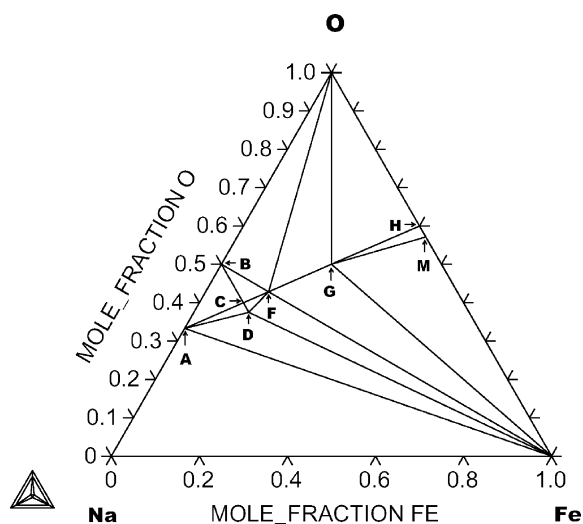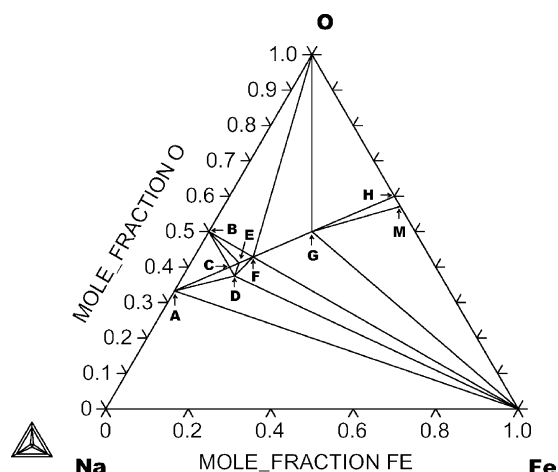

Fig. 3. Isothermal cross-sections of the Na–Fe–O ternary phase diagram in 637–694 K. (A) Na_2O; (B) Na_2O_2; (C) Na_5FeO_4; (D) Na_4FeO_3; (E) $Na_8Fe_2O_7$; (F) Na_3FeO_3; (G) $NaFeO_2$; (H) Hematite; (M) Magnetite.

Predominance diagram on coordinates of $\log P(O_2)$ versus $\log P(Na)$ at 800 K was shown in Fig. 7. It should be noted that the phase Na_4FeO_3(s) only exists at low oxygen potentials compared to the other Na–Fe complex oxides. The calculated highest oxygen potential at 800 K in which Na_4FeO_3(s) can stably exist

Fig. 2. Isothermal cross-sections of the Na–Fe–O ternary phase diagram in 536–637 K. (A) Na_2O; (B) Na_2O_2; (C) Na_5FeO_4; (D) Na_4FeO_3; (F) Na_3FeO_3; (G) $NaFeO_2$; (H) Hematite; (M) Magnetite.
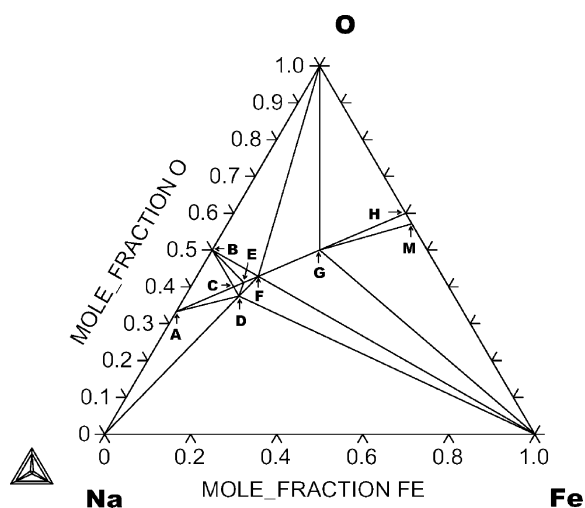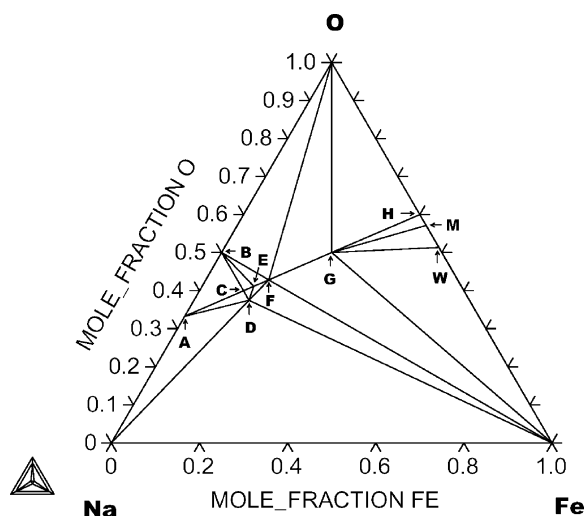

Fig. 4. Isothermal cross-sections of the Na–Fe–O ternary phase diagram in 694–838 K. (A) Na_2O; (B) Na_2O_2; (C) Na_5FeO_4; (D) Na_4FeO_3; (E) $Na_8Fe_2O_7$; (F) Na_3FeO_3; (G) $NaFeO_2$; (H) Hematite; (M) Magnetite.

Fig. 5. Isothermal cross-sections of the Na–Fe–O ternary phase diagram in 838–944 K. (A) Na_2O; (B) Na_2O_2; (C) Na_5FeO_4; (D) Na_4FeO_3; (E) $Na_8Fe_2O_7$; (F) Na_3FeO_3; (G) $NaFeO_2$; (H) Hematite; (M) Magnetite; (W) Wustite.

is as low as about $-536\,kJ\,mol^{-1}$. On the other hand, stable area for $NaFeO_2(s)$ and $Na_3FeO_3(s)$ can be relatively very wide. $Na_8Fe_2O_7$ appears over about 637 K and tends to replace Na_5FeO_4 when temperature is higher than about 944 K. The related transition tem-

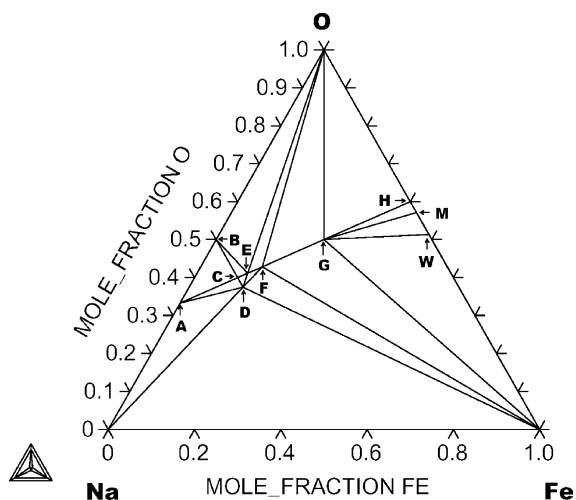Fig. 6. Isothermal cross-sections of the Na–Fe–O ternary phase diagram in 944–1000 K. (A) Na_2O; (B) Na_2O_2; (C) Na_5FeO_4; (D) Na_4FeO_3; (E) $Na_8Fe_2O_7$; (F) Na_3FeO_3; (G) $NaFeO_2$; (H) Hematite; (M) Magnetite; (W) Wustite.
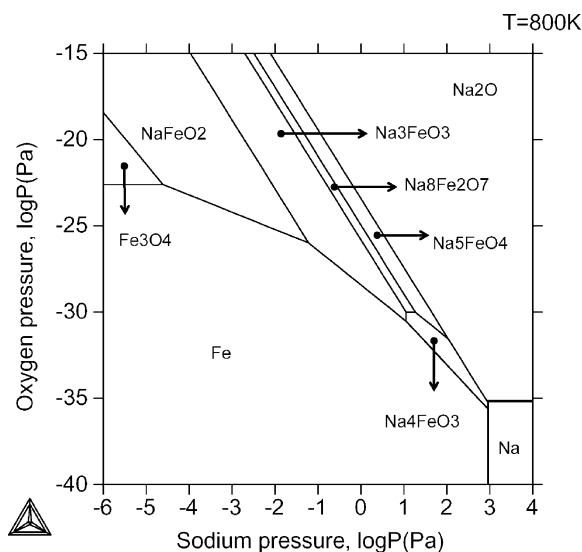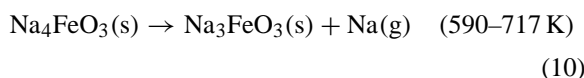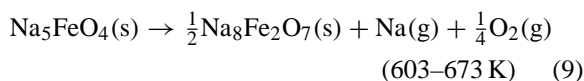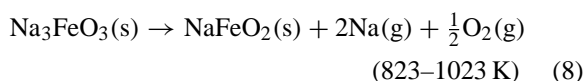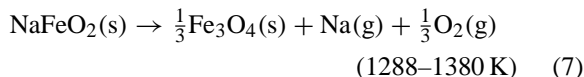

Fig. 7. Predominance diagram of the Na–Fe–O system at 800 K.

peratures are a little hard to be determined precisely because of possible errors in estimating the heat capacities of the corresponding complex oxides. Further experiments were done and the following equilibrium reactions were confirmed by vapor pressure measurements and XRD analysis in the present laboratory.

$$NaFeO_2(s) \rightarrow \tfrac{1}{3}Fe_3O_4(s) + Na(g) + \tfrac{1}{3}O_2(g)$$
$$(1288\text{–}1380\,K) \quad (7)$$

$$Na_3FeO_3(s) \rightarrow NaFeO_2(s) + 2Na(g) + \tfrac{1}{2}O_2(g)$$
$$(823\text{–}1023\,K) \quad (8)$$

$$Na_5FeO_4(s) \rightarrow \tfrac{1}{2}Na_8Fe_2O_7(s) + Na(g) + \tfrac{1}{4}O_2(g)$$
$$(603\text{–}673\,K) \quad (9)$$

$$Na_4FeO_3(s) \rightarrow Na_3FeO_3(s) + Na(g) \quad (590\text{–}717\,K)$$
$$(10)$$

It was a pity that the partial pressures of oxygen in above conditions were too low to be measured by the high temperature mass spectrometer. However, phase identifications, measurements of temperature and partial vapor pressures of sodium provided some experimental evidence that is consistent with the phase diagrams constructed in the present study.

During the phase diagram calculation, it is also found that the phase diagrams are very sensitive to the Gibbs energy of formation of the main ternary Na–Fe oxides. So the assessment of thermodynamic data becomes very important to obtain correct phase diagrams. For example, even a $0.7\,\text{kJ}\,\text{mol}^{-1}$ positive shift in $\Delta_f G^\circ(\text{Na}_4\text{FeO}_3)$ and $\Delta_f G^\circ(\text{Na}_3\text{FeO}_3)$ may refuse coexistence of the two phases and greatly changed the ternary phase diagram. Usually, an experiment error of a few $\text{kJ}\,\text{mol}^{-1}$ seems quite reasonable. It reflects the difficulty of construction of Na–Fe–O phase diagram. This might be the main reason why there exists large discrepancy in the Na–Fe–O phase diagrams published by some pioneers. Fortunately, thermodynamic evaluations of $\text{Na}_3\text{FeO}_3(s)$ in the present study were directly based on the relationship between $\text{Na}_4\text{FeO}_3(s)$ and $\text{Na}_3\text{FeO}_3(s)$ [13]. Thus, the user database can be considered as self-consistent so that calculated phase diagrams constructed seem quite consistent with the experiment results for the time being.

4. Conclusion

Ternary phase diagrams of the Na–Fe–O system are studied from the thermodynamic point of view. By reviewing literature data together with recent DSC and vapor pressure measurements by the present authors, thermodynamic data of main ternary Na–Fe oxides $\text{Na}_4\text{FeO}_3(s)$, $\text{Na}_3\text{FeO}_3(s)$, $\text{Na}_5\text{FeO}_4(s)$ and $\text{Na}_8\text{Fe}_2\text{O}_7(s)$ have been evaluated. New ternary phase diagrams of the Na–Fe–O system have been constructed from room temperature to 1000 K. Environmental effects on stability of the ternary oxides were presented in oxygen–sodium potential diagram at 800 K.

References

[1] W. Dai, S. Seetharaman, L.-I. Staffansson, Scand. J. Metall. 13 (1984) 32.
[2] W. Dai, S. Seetharaman, L.-I. Staffansson, Metall. Trans. B 15 (1984) 319.
[3] T.B. Lindemer, T.M. Besmann, C.E. Jonhson, J. Nucl. Mater. 100 (1981) 178.
[4] S. Seetharaman, S. Du, High Temp. Mater. Proc. 12 (1993) 145.
[5] R. Sridharan, T. Gnanasekaran, C.K. Mathews, J. Alloys Compd. 191 (1993) 9.
[6] R. Sridharan, T. Gnanasekaran, G. Periaswami, C.K. Mathews, in: J. Borgstedt, G. Fress (Eds.), Liquid Metal Systems, Plenum Press, New York, 1995, p. 269.
[7] B. Sundman, B. Jansson, J.-O. Andersson, Calphad 9 (1985) 153.
[8] T.B. Massalski, Binary Alloy Phase Diagram, second ed., 1990, ASM International, Metals Park, OH.
[9] N.P. Bhat, H.U. Borgstedt, J. Nucl. Mater. 158 (1988) 7.
[10] P. Gross, G.L. Wilson, J. Chem. Soc. A (1970) 1913.
[11] B.J. Shaiu, P.C.S. Wu, P. Chiotti, J. Nucl. Mater. 67 (1977) 12.
[12] H. Yokokawa, S. Yamauchi, T. Matsumoto, Themochim. Acta 245 (1994) 45.
[13] J. Huang, T. Furukawa, K. Aoto, Thermochim. Acta, in press.
[14] J.M. Stuve, L.B. Pankratz, D.W. Richardson, Report of investigations 7535, US Department of the Interior, Bureau of Mines, 1971.
[15] R. Sridharan, D. Krishnamurthy, C.K. Mathews, J. Nucl. Mater. 167 (1989) 265.